MOLECULAR IMAGING AND BIOLOGY

Published Online: 2 October 2009

Mol Imaging Biol (2010) 12:259–268
DOI: 10.1007/s11307-009-0267-3

RESEARCH ARTICLE

^{68}Ga-Chloride PET Reveals Human Pancreatic Adenocarcinoma Xenografts in Rats—Comparison with FDG

Tiina Ujula,[1] Satu Salomäki,[1] Anu Autio,[1] Pauliina Luoto,[1] Tuula Tolvanen,[1] Pertti Lehikoinen,[2] Tapio Viljanen,[2] Hannu Sipilä,[1] Pirkko Härkönen,[3] Anne Roivainen[1,4]

[1]*Turku PET Centre, Turku University Hospital, 20521 Turku, Finland*
[2]*Radiopharmaceutical Chemistry Laboratory, Turku PET Centre, Turku, Finland*
[3]*Institute of Biomedicine and MediCity Research Laboratory, University of Turku, Turku, Finland*
[4]*Turku Centre for Disease Modeling, University of Turku, Turku, Finland*

Abstract

Purpose: The aim of the study was to compare ^{68}Ga-chloride with 2-[^{18}F]fluoro-2-deoxy-D-glucose (FDG) for the imaging of pancreatic xenografts.

Procedures: Rats with subcutaneous human pancreatic adenocarcinoma xenografts were evaluated *in vivo* by dynamic positron emission tomography (PET) and *ex vivo* by measuring radioactivity of excised tissues and by digital autoradiography of tumor cryosections.

Results: Both tracers were capable of delineating all subcutaneous tumors from surrounding tissues by PET. The standardized uptake values of tumors by PET were 0.9±0.3 (mean±SD) for ^{68}Ga-chloride (n=13) and 1.8±1.2 for FDG (n=11). *Ex vivo* studies showed tumor-to-muscle ratio of 4.0±0.3 for ^{68}Ga-chloride (n=4) and 7.9±3.2 for FDG (n=4).

Conclusions: ^{68}Ga-chloride delineated subcutaneously implanted pancreatic adenocarcinoma xenografts by PET, but the uptake was lower than FDG. Further studies to clarify the value of ^{68}Ga-chloride for PET imaging of tumors are warranted.

Key words: Gallium-68, Fluorine-18 FDG, PET, Tumor xenografts

Introduction

Gallium-67 citrate (^{67}Ga; $T_{1/2}$=78 h) has been used as an imaging agent in single-photon emission computed tomography (SPECT) for decades for the purpose of detecting certain tumors and infection/inflammation, in spite of its disadvantages resulting mainly from such unfavorable physical characteristics as high radiation exposure and long examination time. The first tumor uptake studies with a positron-emitting gallium-68 (^{68}Ga; $T_{1/2}$=68 min) were performed in the 1960s [1, 2]. For a long period of time, ^{68}Ga was almost forgotten, but during the last years, it has gone through a renaissance. ^{68}Ga has been applied for the labeling of peptides and oligonucleotides with the macrocyclic chelating agent 1,4,7,10-tetraazacyclododecane-*N*,*N*′,*N*″,*N*‴-tetraacetic acid (DOTA) in order to target tumors by positron emission tomography (PET) [3, 4]. Some ^{68}Ga-labeled tumor targeting radiopharmaceuticals, e.g., ^{68}Ga-DOTATOC, ^{68}Ga-DOTANOC, and ^{68}Ga-DOTA-Ianreotide binding to somatostatin receptors, ^{68}Ga-DOTA-bombesin binding to bombesin receptors, and ^{68}Ga-DOTA-D-Glu-gastrin binding to gastrin-releasing peptide receptors, have been reported to be potential imaging agents in clinical studies [5, 6]. Preclinical evaluation of interesting ^{68}Ga-labeled biomolecules, e.g., ^{68}Ga-deferoxamine-folate and ^{68}Ga-DOTA-hEGF, has also been reported [7, 8].

Significance: This is the first study to evaluate ^{68}Ga-chloride for PET imaging of pancreatic xenografts in comparison with FDG.

Correspondence to: Anne Roivainen; *e-mail:* anne.roivainen@utu.fi

2-[^{18}F]Fluoro-2-deoxy-D-glucose (FDG) is the most widely used PET imaging agent. FDG is a glucose analog that reflects the level of glucose metabolism. Glucose consumption is increased in tumors because of rapid cell proliferation. Glucose and FDG uses GLUT-1 and GLUT-3 cell surface transporters, which are overexpressed in cancer cells [9]. FDG, like glucose, is phosphorylated by *hexokinases* (particularly *hexokinase* II) into 2-[^{18}F]fluoro-2-deoxy-D-glucose 6-phosphate (FDG 6-P). Subsequently, FDG 6-P is trapped inside the cell because it is not metabolized any further.

Very recently, we have been able to establish a relationship between the ^{68}Ga-chloride uptake with PET at the site of local bone infection and underlying structural changes determined with peripheral quantitative computed tomography [10]. In addition, when using ^{68}Ga-chloride as a control in our ^{68}Ga-oligonucleotide studies, we noticed uptake in tumors during 2 h PET imaging [4]. The purpose of this study was to preliminarily evaluate if gallium-68 (^{68}Ga) could be used for PET imaging of tumors in a similar fashion as ^{67}Ga is used for SPECT. The advantage of ^{68}Ga-chloride over FDG would be the fast and simple production, i.e., the cyclotron and labeling-free production. ^{68}Ga-chloride is readily available at a PET laboratory. We tested ^{68}Ga-chloride by PET imaging of experimental tumors in comparison with FDG. The results were also verified *ex vivo*. Compared with the use of ^{67}Ga in SPECT, ^{68}Ga-chloride PET would have the following advantages: better spatial resolution, higher sensitivity, possibility for quantitative assessment of tracer accumulation in tissues, and lower absorbed radiation dose for the study subject.

Materials and Methods

Preparation of Tracers

^{68}Ga-chloride was eluted with 0.1 M HCl from a ^{68}Ge/^{68}Ga generator (Cyclotron Co., Obninsk, Russia). The radioactive elution peak, monitored online with a positron-sensitive photodiode detector (Hamamatsu S5591, Hamamatsu Photonics K.K. Solid State Division, Hamatsu City, Japan), was collected, and the ^{68}Ga-chloride was neutralized with 1.0 M NaOH. FDG was prepared as described earlier [11].

Animal Model

The human pancreatic ductal adenocarcinoma cell line, BxPC-3, was purchased from American Type Culture Collection (Rockville, MD, USA). The cells were grown in RPMI 1640 culture medium supplemented (10%) with heat-inactivated fetal bovine serum, 2 mM L-glutamine, 100 U/mL penicillin, and streptomycin (100 μg/mL) in a humidified atmosphere of 5% CO_2 at 37°C. The cells were detached from the culture bottle by trypsin–ethylenediaminetetraacetic acid and resuspended (5×10^7 cells/mL) in medium for implantation.

Twenty-nine athymic male Hsd/RH-rnu/rnu rats were obtained from Harlan (The Netherlands) at the age of 6 weeks. Tumor cells (10^7/rat) were injected subcutaneously into the neck, and tumors were allowed to grow to a size of 1 cm in diameter. All animal studies had been approved by the Lab-Animal Care & Use Committee of the University of Turku.

PET Imaging

To detect the tumor uptake of tracers and to quantify their organ distribution and kinetics, 2 h dynamic PET imaging was performed. Nineteen rats with BxPC-3 xenografts (weight 336±50 g) were anesthetized intraperitoneally with sodium pentobarbital (60 mg/kg; Mebunat, Orion, Finland) or with a mixture of fentanyl citrate plus fluanisone (0.25 and 8.0 mg/kg, respectively; Hypnorm® = fentanyl citrate 0.315 mg/mL and fluanisone 10 mg/mL, Janssen Pharmaceutica, Beerse, Belgium) and midazolam (4.0 mg/kg; Dormicum 5 mg/mL, Roche, Espoo, Finland). The rats were placed in the center of the scanner gantry to obtain the best resolution for small objects and kept on a warm pallet during the imaging procedure. PET imaging was performed either with Advance scanner (GE Medical Systems, Milwaukee, WI, USA) or with HRRT camera (Siemens Medical Solutions, Knoxville, TN, USA) [12, 13].

After transmission scan for attenuation correction, a tracer was injected directly as a bolus intravenously via a tail vein. PET imaging started at the time of injection. The mean±SD dose was 16±3 MBq for ^{68}Ga-chloride (n=13) and 16±9 MBq for FDG (n=11). Prior to tracer injection, rats fasted for at least 2 h. Of a total of 19 rats, five were imaged with both tracers on subsequent days. The acquisition times were 5×60 and 23×300 s, with the total imaging duration being 120 min.

PET data were iteratively reconstructed with the ordered-subsets expectation maximization (OS-EM) algorithm. All PET images were reviewed on computer screen in the transaxial, coronal, and sagittal planes along with maximum-intensity-projection images. Two reviewers aware of subcutaneously implanted tumor xenografts in the neck area independently evaluated tracer uptake both visually and semiquantitatively. The radiotracer uptake in the tumor was visually compared to the surrounding tissue (skin, fat, and muscle) uptake as negative, less-than-surrounding tissue uptake or equivalent-to-surrounding tissue uptake, and positive, uptake which is higher than the surrounding tissue uptake. In case of discrepancies between the two reviewers, a consensus was reached in a joint reading session. Semiquantitative analysis was performed by drawing a standardized circular region of interest (ROI) to the tumor (ROI Ø 5 mm), heart (ROI Ø 6 mm), kidney (ROI Ø 4 mm), liver (ROI Ø 6 mm), and urinary bladder (ROI Ø 4 mm) areas. The heart ROI was drawn to cover the whole heart including both myocardium and the blood pool radioactivity. The average radioactivity concentration in a ROI (kiloBecquerels per milliliter) was used for further analyses. The tracer uptake was reported as mean standardized uptake values (SUV), which was calculated as the radioactivity of the ROI divided by the injected dose per animal body weight. Biokinetic/time–activity curves (TAC), representing the relative radioactivity concentration in the organ of interest (SUV) *vs.* time after injection, were determined accordingly. TACs were decay corrected to the time of injection.

Ex Vivo Measurements

The uptake of ^{68}Ga-chloride and FDG in tumors was studied *ex vivo* in tumor-bearing animals. Eight rats (weight 280±69 g) were anesthetized with a mixture of Hypnorm–Dormicum, as described above and intravenously administered with 12±3 MBq of ^{68}Ga-chloride (n=4) or 15±3 MBq of FDG (n=4). Prior to tracer injection, rats fasted for at least 2 h. Ninety minutes after tracer distribution, a blood sample was obtained via intracardiac puncture, and the animals were killed by intracardiac administration of sodium pentobarbital (Mebunat®, Orion, Finland). The time point for *ex vivo* measurements was based on our

previous studies [10]. Samples of blood, tumor, liver, lung, muscle, and skin were excised, weighed, and measured for total radioactivity in an automated gamma counter (1480 Wizard 3″ Gamma Counter; EG & G Wallac, Turku, Finland) cross-calibrated with a dose calibrator (VDC-202, Veenstra Instruments, Joure, The Netherlands) and PET cameras. The tail was also measured for radioactive content to determine the accuracy of the injections. The radioactivity concentration was decay corrected to the time of injection, the radioactivity remaining in the tail was compensated, and the results were expressed as SUV (organ radioactivity/organ weight)/(total given radioactivity/rat body weight). The radioactivity ratios between the target (tumor) and nontarget (blood, liver, lung, muscle, and skin) organs were also calculated.

Tumor Autoradiography, Histology, and Immunohistochemical Staining

Two rats (weight 224 g and 213 g) were injected with 19 MBq of ^{68}Ga-chloride or 24 MBq of FDG, respectively. After tracer distribution (90 min), the tumors were excised, frozen in dry ice, and cut with a cryomicrotome into 10–20-µm sections. Tumor sections were thaw-mounted onto microscope slides, briefly air dried, and exposed to an imaging plate (Fujifilm BAS TR, Fuji Photo Film Co, Japan) for two half-lives of radio-isotope in question. The distribution of radioactivity in the sections was digitally scanned using a Fuji BAS-5000 device (Fuji Tokyo, Japan) with the image resolution of 25 µm.

After autoradiography, the same sections were stained with hematoxylin and eosin (HE) or using an immunohistochemical method for light microscopy to obtain corresponding histological information. In addition, some tumor samples were fixed with 4% formaldehyde, embedded in paraffin, and cut into 10-µm sections, and the sections were stained with HE. For immunohistochemical staining, DakoCytomation EnVision-system-HRP (K4001, Dako, Glostrup, Denmark) two-step immunohistochemical technique was used.

After ^{68}Ga-chloride autoradiography, the sections were stained with mouse antirat CD68 monoclonal antibody (MCA341GA; AbD Serotec, Oxford, UK; optimal dilution 1:2,000) to examine if the

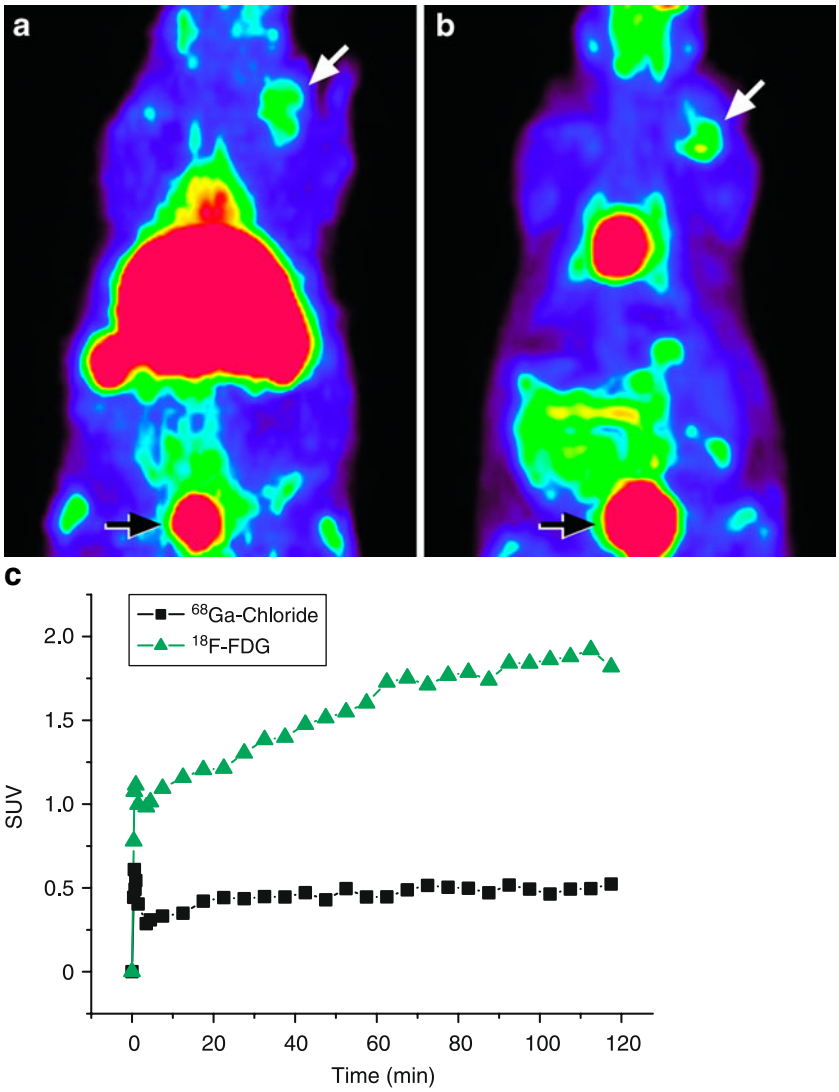

Fig. 1. Coronal PET images of a rat injected with **a** ^{68}Ga-chloride and **b** FDG on subsequent days. Tumor formed by subcutaneously implanted BxPC-3 human pancreatic adenocarcinoma cells is marked with a *white arrow*. Urinary bladder is marked with a *black arrow*. Images (a summation of a 60- to 70-min period after injection) are color-coded according to the level of radioactivity, from *dark blue* (the lowest) to *hot red* (the highest). **c** The tumor uptake (standardized uptake value, *SUV*) of ^{68}Ga-chloride and FDG as a function of time.

Table 1. Uptake of ^{68}Ga-chloride and FDG in human pancreatic adenocarcinoma xenografts in rats by using two different PET devices, i.e., GE Advance and Siemens HRRT

	^{68}Ga-chloride (n=13)		FDG (n=11)	
	GE Advance	Siemens HRRT	GE Advance	Siemens HRRT
Rat # 1	1.0		1.6	
Rat # 2	0.9		1.8	
Rat # 3	1.3		4.9	
Rat # 4	0.7		0.7	
Rat # 5	0.6		1.2	
Rat # 6	1.7			
Rat # 7	0.7			
Rat # 8	0.7			
Rat # 9	0.7			
Rat # 10	0.7			
Rat # 11			1.8	
Rat # 12			1.9	
Rat # 13			1.3	
Rat # 14			0.5	
Rat # 15		0.9		
Rat # 16		0.6		
Rat # 17		0.6		
Rat # 18				3.0
Rat # 19				1.5
Mean±SD	0.9±0.4	0.7±0.2	1.7±1.3	2.3±1.0
Mean±SD (all)	0.9±0.3		1.8±1.2	

Results are expressed as standardized uptake value

radioactivity originates from macrophage uptake. Antibody was located with 3,3′-diaminobenzidine tetrahydrochloride (Liquid DAB Substrate, K3468; Dako, Glostrup, Denmark). Finally, immunohistochemical sections were slightly counterstained with Mayer's hematoxylin, washed, and mounted.

The digital autoradiographs were combined with digital histological and immunohistological images using GIMP 2.4.5 (GNU Image Manipulation Program, authored by Peter Mattis and Spencer Kimball; http://www.gimp.org/) and Hugin 0.7 beta 3 hugin (Hugin, authored by Andrew Mihal, Pablo d'Angelo, Max Lyons, Erik Krause, Konstantin Rotkvich, and Christoph Spiel; http://hugin.sourceforge.net/) softwares. The intratumoral tracer distribution was reviewed on computer screen by two observers.

Statistical Methods

All the results are expressed as mean±SD. After testing of normality and variance, an analysis of variance test was applied to study the significance of differences between the tracers. A t test was used for the comparison of PET and *ex vivo* data. A log transformation because of skeweness was used for all data, except for comparison of *ex vivo* measurements. A P value of less than 0.05 was considered statistically significant. Statistical analyses were conducted using SAS 9.1.3 statistical software (SAS Institute Inc., Cary, NC, USA).

Results

PET Imaging

Both tracers were capable of delineating all subcutaneous BxPC-3 tumor xenografts from surrounding tissues by PET (Fig. 1a, b). Based on 2 h dynamic PET imaging, the peak radioactivity of ^{68}Ga-chloride in the tumor was reached faster in comparison to FDG. The uptake of ^{68}Ga-chloride at the site of tumors showed very fast initial uptake and moderate decline with a plateau at 10 min after injection. In contrast, uptake of FDG accumulated slowly and reached a plateau at 60 min (Fig. 1c). According to PET imaging, the tumor uptake expressed as SUV was 0.9±0.3 for ^{68}Ga-chloride (n=13) and 1.8±1.2 for FDG (n=11; Table 1). The FDG SUV of tumor was significantly higher than that of ^{68}Ga-chloride (P=0.003; Fig. 2). The results obtained by using GE Advance scanner were in accordance with those obtained by using Siemens HRRT camera (P>0.05 for both tracers).

In case of ^{68}Ga-chloride, the excess of radioactivity was distributed into heart, liver, and urinary bladder. The critical organs for FDG distribution were heart and urinary bladder (Fig. 1a, b). The corresponding tissue TACs are shown in Fig. 3.

Ex Vivo Biodistribution

The results of the *ex vivo* measurements are presented in Table 2, and they are in accordance with the results of *in vivo* PET imaging (P>0.05; Fig. 2). The tumor SUV was 0.9±0.2 for ^{68}Ga-chloride and 2.2±1.2 for FDG, and the difference was statistically insignificant (P>0.05).

Target-to-nontarget ratios, i.e., tumor-to-blood, tumor-to-liver, tumor-to-lung, tumor-to-muscle, and tumor-to-skin ratios, are presented in Table 2 and Fig. 4. The tumor-to-blood ratio of ^{68}Ga-chloride was significantly lower compared to FDG (P<0.0001). Both tracers gave tumor-to-muscle ratios high enough to differentiate the tumor from surrounding tissues (range 3.7–4.3 with ^{68}Ga-chloride and 5.7–12.6 with FDG).

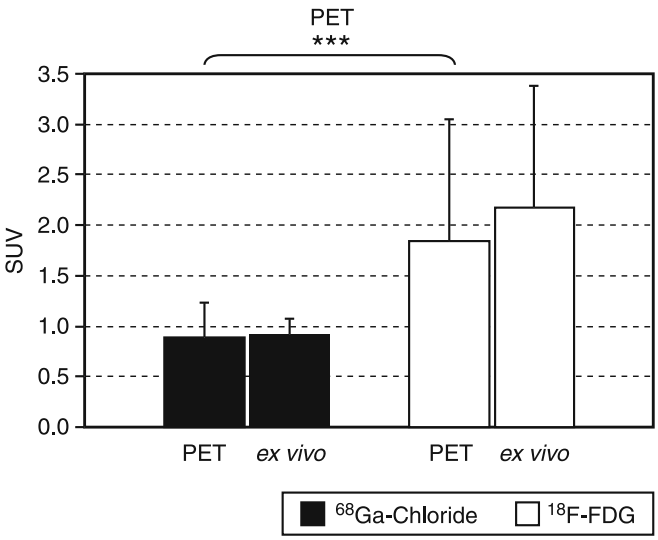

Fig. 2. Standardized uptake values (*SUV*) at tumor site calculated from PET and *ex vivo* biodistribution data. The results of the *ex vivo* measurements were in accordance with the results of *in vivo* PET imaging. ***P<0.005.

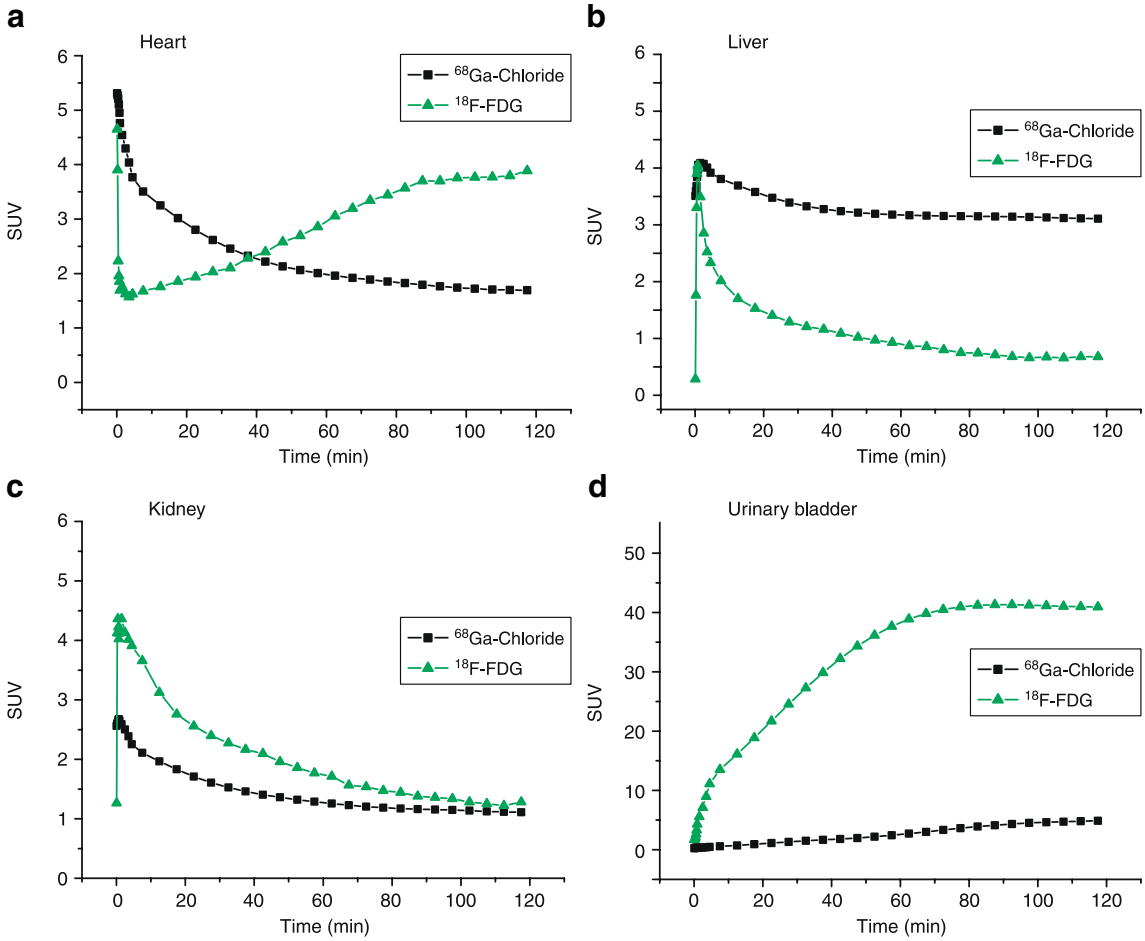

Fig. 3. *In vivo* biokinetics (amount of radioactivity *vs.* time after injection) of intravenously administered ^{68}Ga-chloride and FDG in the rat's **a** heart, **b** liver, **c** kidney, and **d** urinary bladder. Radioactivity concentrations are expressed as standardized uptake values (*SUV*) *vs.* time after injection (minute). Mean value of 11 to 13 experiments.

Tumor Autoradiography, Histology, and Immunohistochemical Staining

Representative digital autoradiographs of ^{68}Ga-chloride and FDG distribution in the tumor tissue are shown in Fig. 5. The imaging agents showed different biodistribution within the tumor. The ^{68}Ga radioactivity was quite homogeneously distributed, while distribution of FDG was more heterogenous.

The histological sections of BxPC-3 tumors showed mainly homogenous, viable tumor tissue without any major necrotic areas (Fig. 6). ^{68}Ga-chloride uptake by the tumor

Table 2. *Ex vivo* biodistribution of intravenously administered ^{68}Ga-chloride and FDG in tumor-bearing rats

	Blood	Liver	Lung	Muscle	Skin	Tumor	T/B	T/Li	T/Lu	T/M	T/S
^{68}Ga-chloride (n=4)											
Rat # 20	2.7	6.7	3.0	0.3	0.5	1.0	0.4	0.2	0.4	4.0	2.2
Rat # 21	2.4	8.6	1.5	0.2	0.5	0.9	0.4	0.1	0.6	3.8	1.8
Rat # 22	2.5	7.1	1.9	0.2	0.7	1.0	0.4	0.1	0.6	4.3	1.5
Rat # 23	3.0	1.1	1.0	0.2	0.5	0.7	0.2	0.7	0.7	3.7	1.5
Mean ± SD	2.7±0.3	5.9±3.3	1.9±0.8	0.2±0.03	0.5±0.1	0.9±0.2	0.3±0.1	0.3±0.3	0.5±0.1	4.0±0.3	1.8±0.4
Range	2.4–3.0	1.1–8.6	1.0–3.0	0.2–0.3	0.5–0.7	0.7–1.0	0.2–0.4	0.1–0.7	0.4–0.7	3.7–4.3	1.5–2.2
FDG (n=4)											
Rat # 24	0.5	0.7	2.3	0.4	1.6	3.2	5.8	4.8	1.4	7.2	1.9
Rat # 25	0.8	1.1	2.2	0.5	1.5	3.1	3.6	2.9	1.4	6.0	2.1
Rat # 26	0.4	0.5	1.0	0.3	1.1	1.9	5.1	4.0	1.8	5.7	1.8
Rat # 27	0.1	0.1	0.2	0.04	0.2	0.6	8.8	7.4	3.4	12.6	3.4
Mean ± SD	0.5±0.3	0.6±0.4	1.4±1.0	0.3±0.2	1.1±0.7	2.2±1.2	5.8±2.2	4.8±1.9	2.0±0.9	7.9±3.2	2.3±0.7
Range	0.1–0.8	0.1–1.1	0.2–2.3	0.0–0.5	0.2–1.6	0.6–3.2	3.6–8.8	2.9–7.4	1.4–3.4	5.7–12.6	1.8–3.4

Results are expressed as standardized uptake value
T/B tumor/blood, *T/Li* tumor/liver, *T/Lu* tumor/lung, *T/M* tumor/muscle, *T/S* tumor/skin

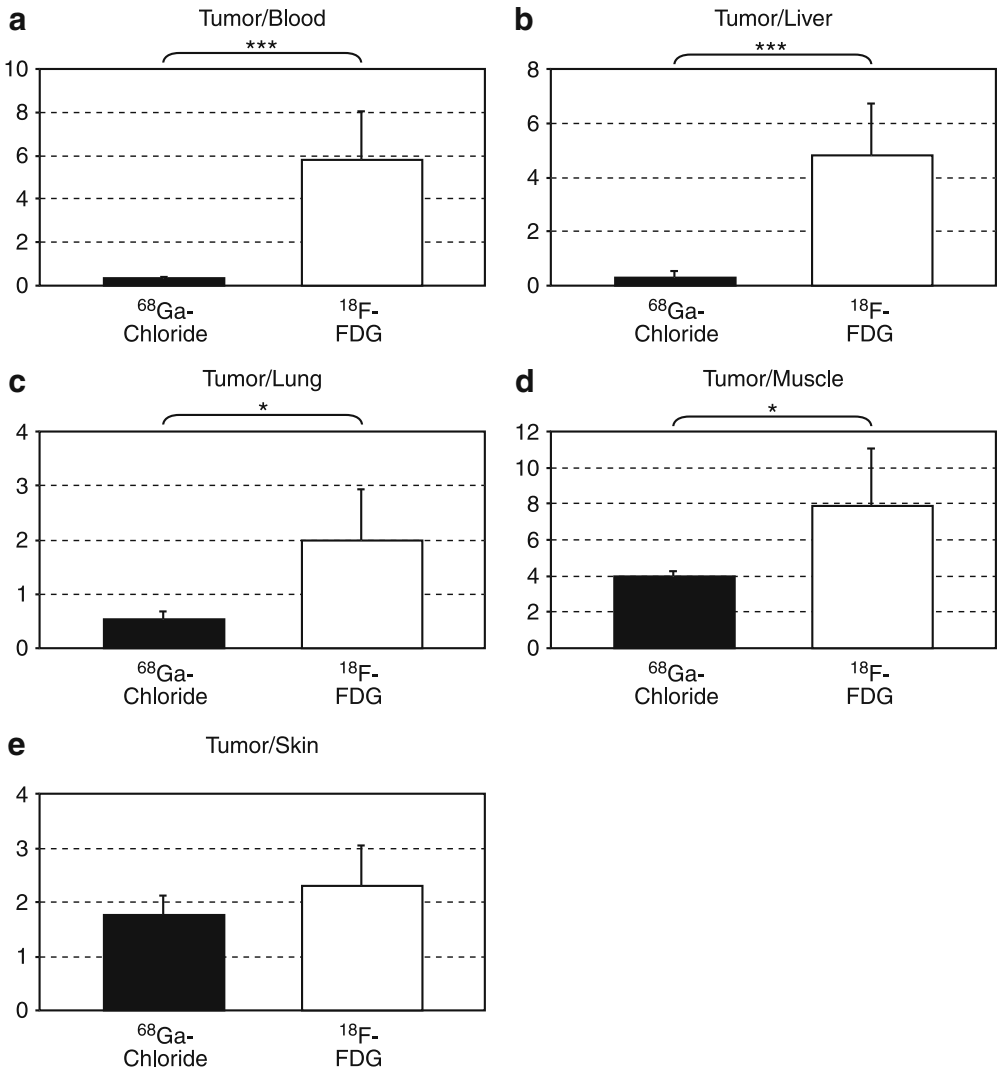

Fig. 4. **a** Tumor-to-blood, **b** tumor-to-liver, **c** tumor-to-lung, **d** tumor-to-muscle, and **e** tumor-to-skin ratios calculated from the *ex vivo* measurements of ^{68}Ga-chloride and FDG at 90 min after injection in tumor bearing athymic rats. *$P<0.05$; ***$P<0.005$.

was mostly by viable cancer cell islets. Immunohistochemical staining with mouse antirat CD68 recognizing rat macrophages revealed homogenous distribution in the tumor tissue (Fig. 7).

Discussion

This experimental study was designed to investigate the feasibility of ^{68}Ga-chloride for PET imaging of tumors by comparing it with FDG. Although FDG is a widely used imaging agent in PET and ^{67}Ga-citrate in SPECT, comparison with ^{68}Ga-chloride has not been performed earlier. Our results revealed that ^{68}Ga-chloride was able to differentiate experimental tumors from surrounding tissues (Fig. 1). The tumor uptake of ^{68}Ga-chloride was lower than that of FDG (Table 1; Fig. 2).

Human pancreatic adenocarcinoma xenograft in rat was chosen for an experimental tumor model, since imaging and early diagnosis of pancreatic cancer still remains a challenge [14, 15]. One problem that hinders early diagnosis is that only symptomatic patients with suspected malignancy are PET imaged. PET is not the primary method for diagnosis, even though it has been reported to be the most accurate one [15]. Since the production of ^{68}Ga-chloride is cyclotron-free, ^{68}Ga-chloride PET might facilitate the availability of PET in centers where no cyclotron is available.

Both tested tracers were capable of visualizing subcutaneous tumors (Fig. 1). According to dynamic PET imaging, the tumor uptake of ^{68}Ga-chloride was much faster than the uptake of FDG. Blood clearance of ^{68}Ga radioactivity estimated from TAC of heart was slower compared with FDG (Fig. 3a), which is in accordance to the fact that Ga^{3+} binds to transferrin. The slow clearance was seen also as the low tumor-to-blood ratio of ^{68}Ga-chloride as noticed by *ex vivo* studies (Table 2; Fig. 4a). In our previous studies, the ^{68}Ga-chloride uptake to healthy rat pancreas was low (SUV

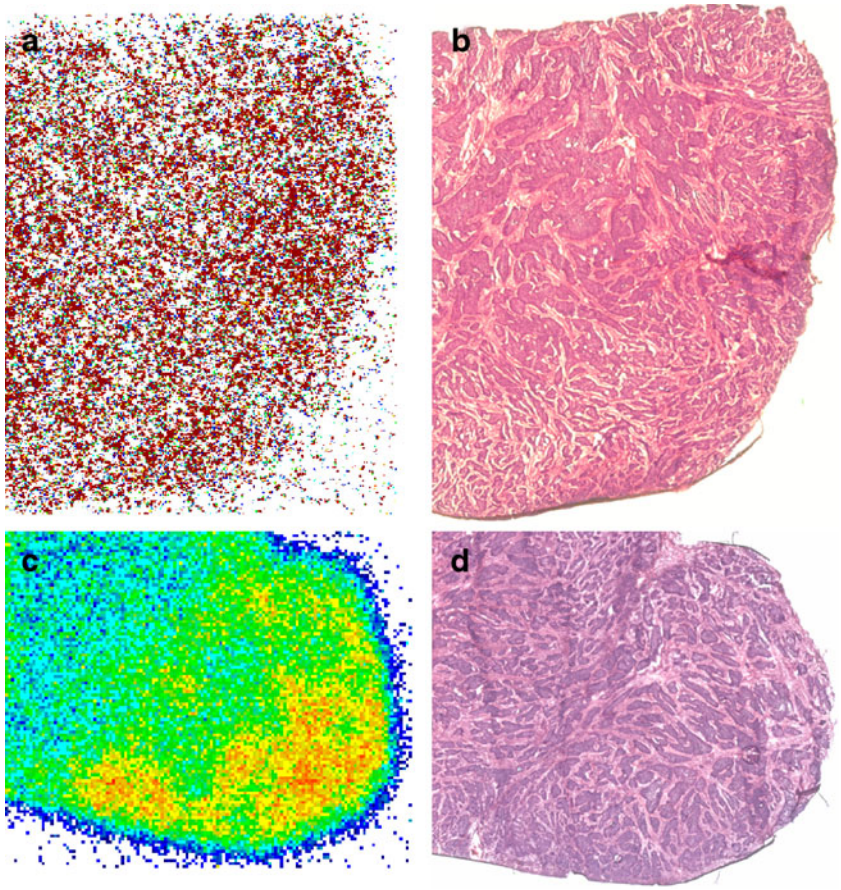

Fig. 5. Representative digital autoradiographs of BxPC-3 tumor cryosections and corresponding hematoxylin and eosin stainings. **a** ^{68}Ga-chloride autoradiography at 90 min postinjection (p.i.) and **b** the HE-staining of the same section. **c** FDG autoradiography at 90 min p.i. and **d** the corresponding HE staining. The *dark blue* represents the lowest and *hot red* the highest amount of radioactivity.

0.4±0.1 at 2 h after injection) [16]. When tumor uptake was compared to the muscle, both ^{68}Ga-chloride and FDG had ratio ≥4 (Table 2; Fig. 4d). However, there was a great variation in FDG accumulation in tumor xenografts between animals. We used skin as another background tissue because tumor cells were subcutaneously transplanted. In general, the determination of true skin radioactivity is difficult, since hair and subcutaneous fat may interfere with the results if not carefully removed from the skin sample. Tumor-to-lung and tumor-to-liver ratios are valuable when evaluating the potential of a new imaging agent to differentiate tumors/metastases from these tissues. Pancreatic cancer cells easily send metastases, in particular, to the liver after surgical operation [14], and many cancers, like breast cancer, are

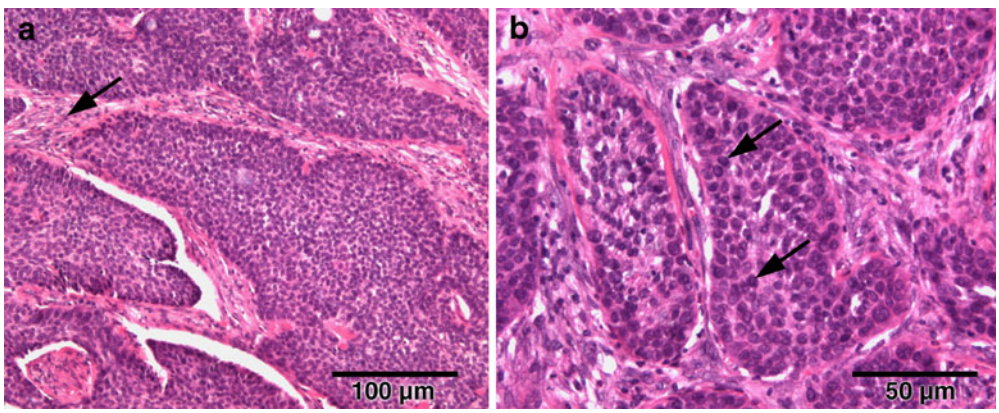

Fig. 6. Hematoxylin and eosin stained paraffin sections of BxPC-3 tumor. **a** Tumor tissue is viable and without major necrotic areas. Stroma is marked with an *arrow*. *Bar*=100µm. **b** BxPC-3 pancreatic adenocarcinoma cells form follicular structures (*arrows*). *Bar*=50µm.

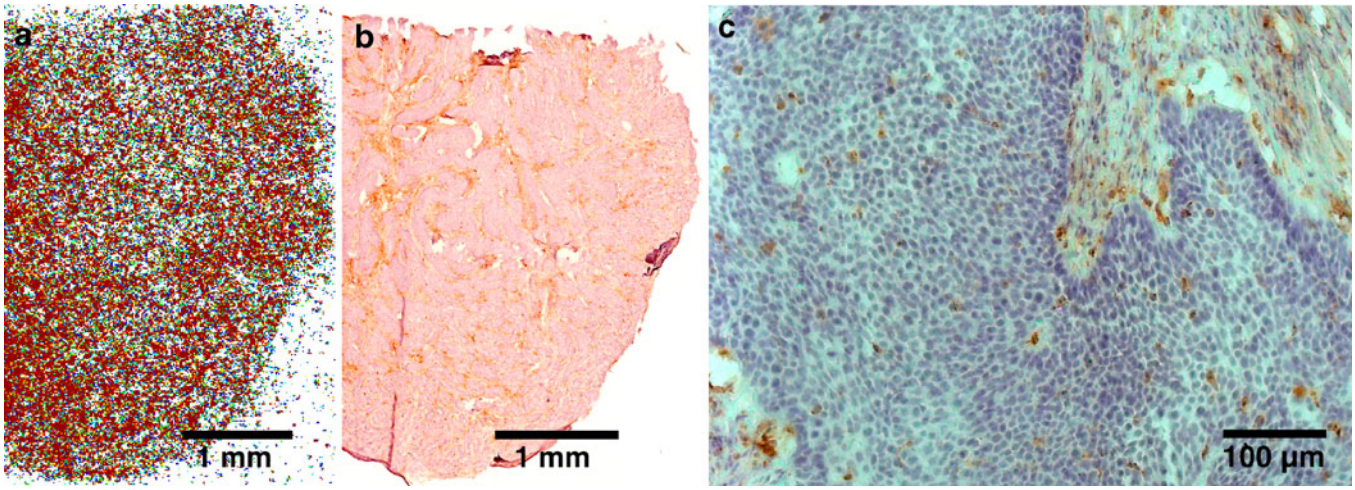

Fig. 7. Representative digital autographs and immunohistological stainings of BxPC-3 tumor cryosections. **a** ^{68}Ga-chloride autoradiography, **b** macrophage staining with CD68 antibody, and **c** magnification (×120) of the same section show rather uniform distribution of the radioactivity and macrophages, respectively. The CD68 positive staining is strong also in the stroma.

known to send metastases to the lungs [17]. From the tested tracers, FDG seems to be clearly superior to differentiate tumors from the normal liver tissue (Table 2; Fig. 4b). FDG seems the best in visualizing tumors in the lungs also. Identification of tumors with ^{68}Ga-chloride in the abdominal area might be challenging due to high blood pool and liver radioactivity, although use of magnetic resonance imaging (MRI) or CT as an anatomical reference to PET might help.

Despite technological advances, PET is characterized by a relatively low spatial resolution. In this work, we used clinical PET devices (GE Advance and Siemens HRRT) for the imaging of rat because at the time of the study, we did not have access to a dedicated small animal PET scanner. The animal was placed in the center of the scanner gantry giving the highest possible spatial resolution, i.e., 4.8 mm with GE Advance and 2.7 mm with Siemens HRRT. Unfortunately, the structures we were aiming at were quite small (tumor diameter approximately 10 mm), which might result in partial-volume effect (PVE) and possibly invalidate the *in vivo* quantitative PET data. PVE means that the apparent pixel values in PET images are influenced by the surrounding high pixel values [18]. In the present study, the central 200-mm-diameter transaxial field of view was reconstructed using OS-EM algorithm [19]. Using the 128×128 matrix, this leads to the pixel size of 1.56×1.56 mm, which is approximately one third (GE Advance) or half (Siemens HRRT) of the image resolution. Boellaard *et al.* have obtained superior image quality by using OS-EM reconstruction instead of filtered back-projection, resulting in lower PVE [20]. In theory, PVE correction is possible if high-resolution structural imaging, such as magnetic resonance imaging, can be coupled with the information of the scanner resolution. However, lack of anatomic MRI of the rats prevented PVE correction in this study. To minimize the PVE, we used the average radioactive concentration within the ROI (kiloBecquerels per milliliter).

The majority of positron-emitting radionuclides are produced by expensive accelerators requiring qualified personnel. ^{68}Ga offers a cyclotron-independent, convenient, and low-cost access to PET radiopharmaceuticals. ^{68}Ga is readily available by elution from ^{68}Ge/^{68}Ga generator possessing 1–2 years life span depending on uploaded ^{68}Ge radioactivity. Furthermore, ^{68}Ga has convenient characteristics for PET detection: β+ decay 89%, $E\beta$+max 1.9 MeV, and $T_{1/2}$ 68 min. It has been shown that the clinical image qualities of ^{68}Ga-tracers and ^{18}F-tracers (β+decay 97%, $E\beta$+max 0.64 MeV, $T_{1/2}$ 110 min) are not necessarily very much different from each other [21]. Although the half-life of ^{68}Ga is shorter compared to that of ^{18}F, the significant advantage for ^{18}F-tracers is the lower radiation dose due to their lower positron energy. The ^{68}Ge/^{68}Ga generator supplied by Cyclotron Co., which was used in this study, contains ^{68}Ge attached to a column of an inorganic matrix-based titanium dioxide (TiO_2). Several research groups that are currently using this generator type have reported that the ^{68}Ge breakthrough is <0.01%, and concentration of other metal ions (Zn^{2+}, Al^{3+}, Ge^{4+}, Ti^{4+}, Cu^{2+}) is <50nM in the ^{68}Ga-eluate [3, 22–24].

When ^{68}Ga is eluted from ^{68}Ge/^{68}Ga generator with 0.1 M HCl, it is in the form of $^{68}GaCl_3$. At least some of the ^{68}Ga is hydrolyzed after neutralization with NaOH *in situ* or after administration *in vivo*. In general, in aqueous solution, ^{68}Ga is in the form of a soluble anion called gallate, $^{68}Ga(OH)_4^-$, and/or insoluble neutral hydroxide colloids, $^{68}Ga(OH)_3$, depending on pH and the concentration of ^{68}Ga [24]. The ^{68}Ga radioactivity can migrate in the blood circulation as free $^{68}Ga^{3+}$ or $^{68}Ga^{3+}$ bound to transferrin, ferritin, or lactoferrin after rapid intravenous administration to the vascular system. ^{67}Ga is injected as citrate for SPECT imaging. Since the citrate is only a weak chelator *in vivo*, $^{67}Ga^{3+}$ cation is rapidly released, hydrolyzed, and/or bound to transferrin and other plasma proteins. Because the citrate is able to prevent precipitation of $^{67}Ga(OH)_3$, it is assumed that only a soluble $^{67}Ga(OH)_4^-$ is formed *in vivo*. The use of ^{67}Ga-citrate has been characterized by its slow accumulation in tumors, which makes the imaging of tumors by SPECT possible only after several hours, even

days. In contrast, when using ^{68}Ga-chloride for PET, we observed rapid localization of radioactivity in the target. The form of ^{68}Ga, i.e., the ratio of ^{68}Ga-gallate and ^{68}Ga-hydroxide colloids, was not studied in this study.

The uptake mechanisms of radiogallium into tumors are not fully understood, and a wide variety of factors are involved. It is known that Ga^{3+} behaves *in vivo* similarly to Fe^{3+} by binding to transferrin and using the same transporters [25]. Gallium seems to concentrate in tissues having high concentration of transferrin or transferrin receptors, lactoferrin, or ferritin. All nucleated cells of the body express transferrin receptors at different concentrations. Malignant cells generally express high levels of transferrin receptors because they divide and require iron for DNA synthesis. However, there is some evidence that Ga can also enter tumor cells by transferrin-independent mechanisms. This may be due to a very small soluble gallate ion, $Ga(OH)_4^-$, or a neutral insoluble, $Ga(OH)_3$, both hydrolysis products of Ga [25]. In this study, ^{68}Ga radioactivity seemed to be taken up mostly by viable cancer cell islets according to ^{68}Ga autoradiography and HE staining (Fig. 5). The comparison of autoradiography and CD68 immunohistochemical staining (Fig. 7) suggests that the uptake might also be a result of macrophage phagocytosis. The resolution of autoradiography is not high enough to show the radioactivity uptake of individual cells, but it rather shows the accumulation in certain tissue areas, like tumor cell islets. It is possible that the ^{68}Ga radioactivity is taken up by both tumor cells and infiltrating macrophages. Indeed, accumulation of Ga in macrophages, leukocytes, and bacteria has been reported [26, 27].

Fast tumor uptake of ^{68}Ga-chloride would facilitate PET imaging as soon as 2 h after injection *vs.* long-lasting study procedure with ^{67}Ga-citrate in SPECT imaging, although the slow blood clearance of ^{68}Ga-chloride suggests for a later time point. At 2 h after injection, the high blood pool radioactivity may contribute to tumor uptake as well.

Conclusions

^{68}Ga-chloride and FDG PET imaging were able to delineate subcutaneously implanted human pancreatic adenocarcinoma xenografts in rats. The tumor uptake of FDG was clearly superior, but there was great variation between the animals. ^{68}Ga-chloride showed fast tumor uptake, high blood pool radioactivity, and low urinary excretion. Advantageously, ^{68}Ga-chloride is readily available from a generator system and produces good PET image quality. However, further studies are needed to clarify the value of ^{68}Ga-chloride for PET imaging of tumors.

Acknowledgments. We acknowledge Maija-Liisa Hoffren (SafetyCity Oy Ltd, Turku), Irina Lisinen (Research Centre of Applied and Preventive Cardiovascular Medicine, University of Turku), Jouko Sandholm (Cell Imaging Core, Turku Centre for Biotechnology), and Erica Nyman (Turku Centre for Disease Modeling, University of Turku) for excellent technical assistance. The study was conducted within the Finnish Centre of Excellence in Molecular Imaging in Cardiovascular and Metabolic Research supported by the Academy of Finland, University of Turku, Turku University Hospital, and Abo Academy University. In addition, study was financially supported by grants from the Academy of Finland (nos. 205757 and 103032), the Foundation for the Finnish Cancer Institute, the Instrumentarium Foundation, and the Eli Lilly Foundation. Tiina Ujula and Anu Autio are Ph.D. students supported by the Drug Discovery Graduate School of the University of Turku.

References

1. Anger HO, Gottschalk A (1963) Localization of brain tumors with the positron scintillation camera. J Nucl Med 77:326–330
2. Shealy CN, Aronow S, Brownell GL (1964) Gallium-68 as a scanning agent for intracranial lesions. J Nucl Med 21:161–167
3. Meyer GJ, Mäcke H, Schuhmacher J, Knapp WH, Hofmann M (2004) ^{68}Ga-labelled DOTA-derivatised peptide ligands. Eur J Nucl Med Mol Imaging 31:1097–1104
4. Roivainen A, Tolvanen T, Salomäki S et al (2004) ^{68}Ga-labeled oligonucleotides for *in vivo* imaging with PET. J Nucl Med 45:347–355
5. Henze M, Schuhmacher J, Hipp P et al (2001) PET imaging of somatostatin receptors using ^{68}Ga-DOTA-D-Phe1-Tyr3-octreotide: first results in patients with meningiomas. J Nucl Med 42:1053–1056
6. Maecke HR, André JP (2007) ^{68}Ga-PET radiopharmacy: a generator-based alternative to ^{18}F-radiopharmacy. In: Schubiger PA, Lehmann L, Friebe M (eds) PET chemistry, the driving force in molecular imaging. Springer, New York, pp 215–241
7. Mathias CJ, Lewis MR, Reichert DE et al (2003) Preparation of ^{66}Ga- and ^{68}Ga-labeled Ga(III)-deferoxamine-folate as potential folate-receptor-targeted PET radiopharmaceuticals. Nucl Med Biol 30:725–731
8. Velikyan I, Sundberg AL, Lindhe O et al (2005) Preparation and evaluation of (^{68})Ga-DOTA-hEGF for visualization of EGFR expression in malignant tumors. J Nucl Med 46:1881–1888
9. Younes M, Brown RW, Stephenson M, Gondo M, Cagle PT (1997) Overexpression of Glut1 and Glut3 in stage I non-small cell lung carcinoma is associated with poor survival. Cancer 80:1046–1051
10. Mäkinen TJ, Lankinen P, Pöyhönen T, Jalava J, Aro HT, Roivainen A (2005) Comparison of (^{18})F-FDG and (^{68})Ga PET imaging in the assessment of experimental osteomyelitis due to Staphylococcus aureus. Eur J Nucl Med Mol Imaging 32:1259–1268
11. Hamacher K, Coenen HH, Stocklin G (1986) Efficient stereospecific synthesis of no-carrier-added 2-18F-fluoro-2-deoxy-D-glucose using aminopolyether supported nucleophilic substitution. J Nucl Med 27:235–238
12. DeGrado TR, Turkington TG, Williams JJ, Stearns CW, Hoffman JM, Coleman RE (1994) Performance characteristics of a whole-body PET scanner. J Nucl Med 35:1398–1406
13. Wienhard K, Schmand M, Casey ME et al (2002) The ECAT HRRT: performance and first clinical application of the new high resolution research tomograph. IEEE Trans Nucl Sci 49:104–110
14. Nakao A, Fujii T, Sugimoto H et al (2006) Oncological problems in pancreatic cancer surgery. World J Gastroenterol 12:4466–4472
15. Saif MW, Cornfeld D, Modarresifar H, Ojha B (2008) FDG positron emission tomography CT (FDG-PET-CT) in the management of pancreatic cancer: initial experience in 12 patients. J Gastrointestin Liver Dis 17:173–178
16. Lendvai G, Velikyan I, Bergström M et al (2005) Biodistribution of ^{68}Ga-labelled phosphotiester, phosphorothioate, and 2′-*O*-methyl phosphodiester oligonucleotides in normal rats. Eur J Pharm Sci 26:26–38
17. Minn AJ, Gupta GP, Padua D et al (2007) Lung metastasis genes couple breast tumor size and metastatic spread. PNAS 104:6740–6745
18. Hoffman EJ, Huang SC, Phelps ME (1979) Quantitation in positron emission computed tomography: 1. Effect of object size. J Comput Assist Tomogr 3:299–308
19. Visvikis D, Cheze-LeRest C, Costa DC, Bomanji J, Gacinovic S, Ell PJ (2001) Influence of OSEM and segmented attenuation correction in the

calculation of standardised uptake values for [^{18}F]FDG-PET. Eur J Nucl Med 28:1326–1335
20. Boellaard R, van Lingen A, Lammertsma AA (2001) Experimental and clinical evaluation of iterative reconstruction (OSEM) in dynamic PET: quantitative characteristics and effects on kinetic modeling. J Nucl Med 42:808–817
21. Sanchez-Crespo A, Andreo P, Larsson SA (2004) Positron flight in human tissues and its influence on PET image spatial resolution. Eur J Nucl Med Mol Imaging 31:44–51
22. Velikyan I, Lendvai G, Välilä M et al (2004) Microwave accelerated ^{68}Ga-labelling of oligonucleotides. J Label Compd Radiopharm 47:79–89
23. Breeman WA, de Jong M, de Blois E, Bernard BF, Konijnenberg M, Krenning EP (2005) Radiolabelling DOTA-peptides with ^{68}Ga. Eur J Nucl Med Mol Imaging 32:478–485
24. Hnatowich DJ (1977) A review of radiopharmaceutical development with short-lived generator-produced radionuclides other than ^{99m}Tc. Int J Appl Radiat Isot 28:169–181
25. Weiner RE (1996) The mechanism of ^{67}Ga in malignant disease. Nucl Med Biol 30:70–79
26. Bernstein LR (1998) Mechanisms of therapeutic activity for gallium. Pharmacol Rev 50:665–682
27. Clausen J, Edeling C-J, Fogh J (1974) ^{67}Ga binding to human serum proteins and tumor components. Cancer Res 43:1931–1937